Reply to RC1

In the following, the referee's comments are reproduced (black) along with our replies (blue) and changes made to the text (red) in the revised manuscript. Lines numbers are referring to the unrevised version of the manuscript.

Review:

This work presented the "NOyBOx", a new instrumental framework combining measurements of NO, NO_2 and NO_y from commercial analyzers with a custom-built incoherent broadband cavity-enhanced absorption spectrometer (IBBCEAS) that measures NO_3 and N_2O_5. The design of the IBB-CEAS subsystem, characterize the TDI, cavity optics, transmission losses, were described. Furthermore, a synthetic spectra simulation approach was used to correct the bias of ambient NO_2 and water vapor on concentration retrieval procedure. The first field deployment during the Atmospheric ChemistRy of the Suburban foreSt (ACROSS) campaign was presented.

This work has certain research significance and value. However, there are some problems in the article, please give a supplement. I suggest that the article be published after revision.

We thank the referee for the positive evaluation of our manuscript and for the provision of thoughtful comments.

Major comments:

1. The authors presented the "NOyBOx", a new instrumental framework combining measurements of NO, NO_2 and NO_y from commercial analyzers with a custom-built incoherent broadband cavity-enhanced absorption spectrometer (IBBCEAS) for NO_3/N_2O_5 detection. However, the introduction does not draw a sufficiently clear distinction from previously published multi-channel IBBCEAS and TD-CRDS works that simultaneously measure NO_3/N_2O_5 together with NO_y. Please explicitly state in the manuscript the innovations or optimizations of NOyBOx relative to prior comparable instruments.

We thank the reviewer for this comment. We agree that the original introduction focused primarily on the motivation for combining NO_3/N_2O_5 and NO_y measurements, without sufficiently highlighting the specific configuration and contributions of NOyBOx relative to previously published instruments. In particular, we have not discussed the NOAA six-channel CRDS instrument as detailed in Brown et al. (2017), which combines measurements of N_2O_5, NO, NO_2, total NO_y, NO_3, and O_3. While this instrument provides an impressive range of measurements, it relies on six custom-built CRDS channels and was developed by integrating two previously separate cavity systems and the NO_3 measurement was not successful during that deployment. In contrast, NOyBOx combines custom-built CEAS cavities with commercial analyzers, potentially offering a simpler and less costly approach to obtaining these

measurements. We have revised the final paragraph of the introduction to clarify the instrument's configuration and its main contributions in L135:

Previous multi-channel instruments have combined NO_3/N_2O_5 measurements with measurements of selected additional nitrogen species, such as organic nitrates and NO_2 (Kennedy et al., 2011; Sobanski et al., 2016), or measured total NO_y without speciated NO_3/N_2O_5 measurements (Friedrich et al., 2020; Wild et al., 2014). One exception is a six-channel CRDS instrument as detailed in Brown et al. (2017), which included channels for O_3, N_2O_5, NO, NO_2, and total NO_y, as well as NO_3, although NO_3 measurements were not successfully obtained during that deployment. NOyBOx combines two custom optical cavities for NO_3/N_2O_5 measurements with commercial analyzers for NO_x species and total NO_y. This configuration provides the combined measurements needed to investigate the role of nocturnal oxidation processes in the reactive nitrogen budget that remains barely accessible with isolated measurements, while potentially reducing instrument complexity and cost compared with an approach based entirely on custom CRDS channels.

2. In Section 2.2.2, the authors state that two high-reflectivity mirrors used have a reflectivity of 99.98 ± 0.01 % at 630–690 nm, and separated by 61.5 cm. In previous studies, high-reflectivity mirrors for this spectral band can achieve reflectivity above 99.998 %, or the effective optical path length can be increased by extending the mirror-to-mirror distance to improve the technique's sensitivity. Please elaborate how the detection limits of 1.5 and 2.2 pptv (1σ, 15 s) are achieved under the given experimental conditions.

The detection limit depends not only on the effective optical path length (scaling with mirror reflectivity and mechanical distance), but also on the transmitted intensity, measurement noise, baseline stability, and integration time. Note that higher mirror reflectivity reduces the intensity reaching the detector. Depending on the dominant noise source, the gain in effective path length may therefore be partly or fully cancelled out by the loss in signal-to-noise ratio, so that the LOD does not necessarily improve (see e.g. Vaughan et al., 2008). The selected mirror reflectivity and cavity length represent a compromise between sensitivity, transmitted intensity, mechanical stability and cost. The resulting detection limits of 1.5 pptv for NO_3 and 2.2 pptv for N_2O_5 at 15 s integration time appear reasonable overall in comparison with previously reported instruments, particularly considering that the 15 s integration time corresponds to the optimum averaging time identified by our Allan deviation analysis (see section 3.5.1). Indeed, instruments with comparable detection limits at much shorter integration time (1 s) in Table 1 often have a longer effective path length. We add this point in L492:

Comparable or lower LODs at shorter integration times, as for example reported by Kennedy et al. (2011) and Nam et al. (2022), often go hand in hand with longer effective path lengths achieved through mirrors with higher reflectivity. However, higher mirror reflectivity reduces the intensity reaching the detector, so that increasing *R* does not necessarily improve the LOD (Vaughan et al., 2008). Our choice

of mirror reflectivity and cavity length represents a compromise between sensitivity, transmitted intensity, mechanical stability and cost.

3. In Section 3.3, Model 2 introduces an empirical temperature-dependent wall-loss term in the form of a Hill type, $k_9=k_{Hill}(T)$, to reproduce the decrease in the NO_3 signal at high temperatures. An arbitrarily chosen constant background loss (0.1 s^{-1}) between 300 and 373 K, followed by a sigmoidal increase in k_9 to 0.4 s^{-1} between 373 and 473 K to empirically reproduce the observations. It is suggested to add supporting information: literature-reported NO_3 wall loss on PFA tubing under high-temperature conditions, to justify the choice of these empirical parameters.

We chose the background loss of 0.1 s^{-1} based on our own estimation in Fig. 5a, the sigmoidal increase to 0.4 s^{-1} is, as already stated, an empirical fit to the measurement. Observed pseudo-first order loss rates for a gas flowing through a pipe (assuming a laminar flow and no diffusive limitations) mainly depend on the mean velocity of the considered molecule (here NO_3), the radius of the pipe and the uptake coefficient of NO_3 to the surface. Even the latter can vary substantially depending on the coating quality and the chosen material (Liebmann et al., 2017; Schuster et al., 2009). A quantitative comparison between different setups with different surfaces and operated at different conditions therefore appears not appropriate. In order to provide a semi-quantitative assessment, we note that some studies report NO_3 wall loss rates that are 3–4 times higher in heated Teflon (or Teflon-coated) tubes than in their unheated equivalents (Sobanski et al., 2016; Türk et al., 2026) by adding in L360:

The background loss of 0.1 s^{-1} is consistent with the wall loss we estimated for our unheated NO_3 cavity (see below) while the high temperature wall loss of 0.4 s^{-1} appears plausible considering that previous studies report NO_3 wall loss rates that are 3–4 times higher in heated Teflon (or Teflon-coated) tubes than in their unheated equivalents (Sobanski et al., 2016; Türk et al., 2026).

4. In Section 3.5.1, to investigate the effects of NO_2 and H_2O, a synthetic-spectrum approach used to characterize fitting bias in other spectroscopic retrievals were inspired. The effective limit-of-detection LOD_{eff} is obtained based on Monte-Carlo simulations to correct LOD_{noise} derived from Allan deviation. It is recommended to quantitatively evaluate the potential bias in LOD_{eff} caused by mirror-reflectivity drift.

We thank the reviewer for this helpful comment. To quantify the potential bias in LOD_{eff} caused by mirror-reflectivity drift, we evaluated the variability of (1−R) from consecutive reflectivity measurements over the entire ACROSS campaign. The relative standard deviation (1σ) is 21 % for the NO_3 channel and 27 % for the N_2O_5 channel. These values represent a conservative upper limit. The cavity mirrors were contaminated and cleaned several times during the campaign, so the values include these step-like changes in addition to gradual drift. We propagated these variabilities into the Allan deviation analysis, assuming these $(1-R)$ errors to be constant. This gives upper limits for the noise-limited LOD of 1.8 pptv (NO_3) and 2.8 pptv (N_2O_5). Combining these with the Monte-Carlo-derived

correction for NO_2 and H_2O interferences yields worst-case effective LODs of 4.0 pptv (NO_3) and 5.8 pptv (N_2O_5). We modified Fig. 6 to show the effect of the (1−*R*) error on LOD_{noise} with shaded areas and updated the caption accordingly. We added in L428:

This analysis assumes that the mirror reflectivity remains constant. Drift effects, contamination and cleaning can additionally lead to a variability in *R*, thereby additionally affecting the LOD. For instance, over the entire ACROSS campaign, the standard deviation (1σ) of (1–*R*) from consecutive reflectivity estimations serving as measure for its variability was 21 % for the NO_3 channel and 27 % for the N_2O_5 channel. Propagating these 1σ variabilities into the Allan deviation analysis gives upper limits for LOD_{noise} of 1.8 pptv (NO_3) and 2.8 pptv (N_2O_5). The effect of the (1–*R*) variability on LOD_{noise} is represented by the shaded areas in Fig. 6.

In L457 we added:

For example, using the upper-limit values of LOD_{noise}, which account for variability in *R* results in worst-case (recall that *R* may fluctuate in both senses) effective LODs of 4.0 pptv (NO_3) and 5.8 pptv (N_2O_5).

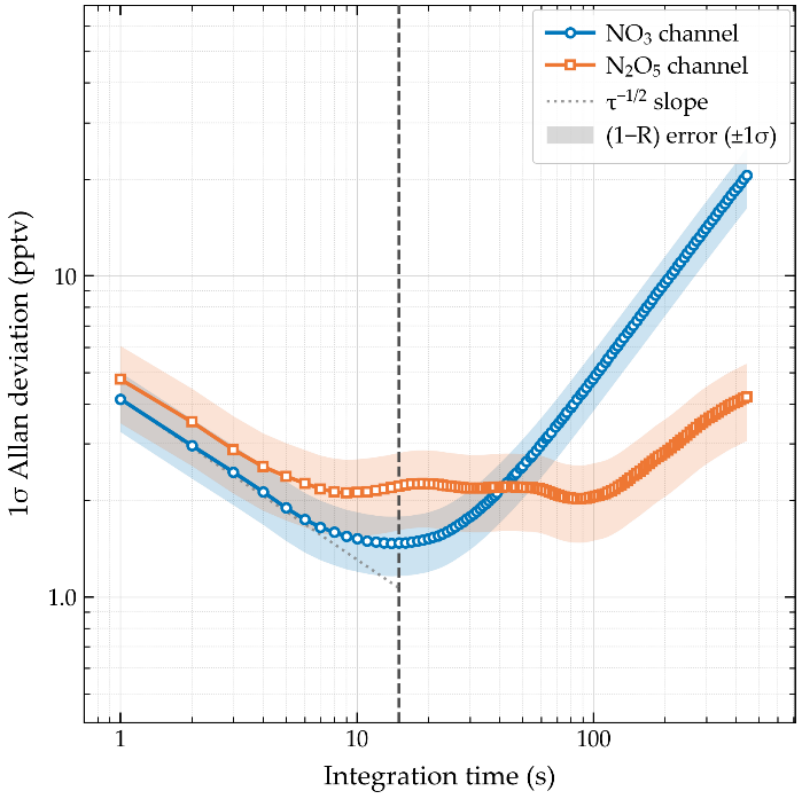


Figure 6. Overlapping Allan deviation (1σ) in dependence of the NO_3 channel's (blue circles) and N_2O_5 channel's (orange squares) integration time. The grey dashed line marks the $1/\sqrt{\tau}$ slope. The vertical black dashed line marks the optimal integration time of 15 s. **The effect of potential variabilities in mirror reflectivity is represented by shaded areas.**

5. In Section 3.4, by repeatedly switching between sampling NO_3 from CESAM through PFA tubing and through the filter, a transmission efficiency (±2σ) was found to be (90 ± 1) %. Please supplement whether this transmission efficiency was obtained using a clean filter or a contaminated filter. Türk et al. (2026), published in AMT, reported that filter exposed to NO_3/O_3 can increase the transmission

efficiency from 70–80 % to approximately 98 %. Please refer to this paper (DOI: 10.5194/amt-19-4815-2026) for details.

This transmission efficiency was obtained using a clean filter. For clarification, we modified the sentence in L380 accordingly:

By repeatedly switching between sampling NO_3 from CESAM through PFA tubing and through a **clean** filter, we found a transmission efficiency (± 2σ) of (90 ± 1) %, thereby confirming previous estimates (Fig. S2).

6. Section 4 stated that "where the observed NO_z increase accounted for only a fraction of the concurrent NO_3/N_2O_5 signal, pointing to additional, yet-unquantified oxidation pathways". It is suggested to briefly list these potential pathways.

Since these pathways are already outlined in the introduction, we prefer to limit our modification to a brief example. We added in L546:

For example, the NO_3-initiated oxidation of BVOCs can lead to the formation of organic nitrates, which themselves may be hydrolysed to contribute to HNO_3 production.

7. Section 3.2 noted that the reflectivity at 662 nm varied between 99.983 % and 99.988 % for the NO_3 channel, corresponding to changes in L by a factor of 0.7. In the field deployment, R and I_0 were determined every 24 h and 1-1.5 h, respectively. It is suggested to add an assessment of the systematic biases for NO_3 and N_2O_5 introduced by the slow drift of R between two successive R-determination events.

This point has already been addressed in our response to comment #4.

8. In Section 2.2.1, precise thermal regulation of the LED light source is mentioned to suppress wavelength drift and intensity instability. It is suggested to supplement information regarding the long-term stability of the central wavelength.

We used the laser emission spectra from our Allan deviation dataset to estimate the stability of the wavelength. We fitted the spectra with Gaussian profiles to estimate the centre wavelengths, calculated the standard deviation which were plotted against time. Linear regression to the data yield negligible drifts (±2σ) of (7.3 ± 7.6) pm h^{-1} and (4.7 ± 3.4) pm h^{-1} for the LED of the NO_3 channel and N_2O_5 channel, respectively. Both values are well below the spectrometer's resolution specified by the manufacturer (> 140 pm). We added in L210:

Under these operating conditions, we observed no statistically relevant long-term drifts in the centre wavelength with values (± 2σ) of (7.3 ± 7.6) pm h^{-1} (NO_3) and (4.7 ± 3.4) pm h^{-1} (N_2O_5), which are below the spectrometer's resolution (> 140 pm, see below).

Additional changes to the manuscript

1. The recommendation for the NO_3–NO_2–N_2O_5 equilibrium constants has been re-evaluated recently in Burkholder et al. (2025), while we still used the outdated expression in Burkholder et al. (2019). We updated K_{eq} in Fig. 9 and the literature list accordingly.
2. The work by Türk et al. (2026) is no longer a preprint, but published in AMT. We updated the reference in the literature list accordingly.
3. In L326, we added the unit of the slope for clarification: Linear regression (solid lines) of the reflectivity yielded (1.18 ± 1.58) x 10^{-8} nm^{-1} x λ + 99.987% and (4.81 ± 0.75) x 10^{-8} nm^{-1} x λ + 99.949%.
4. We accidently omitted the fifth term propagating the error of $T_{N_2O_5}$ in Eq. (6). We corrected the equation accordingly. Note however that we used the correct version of Eq. (6) to calculate the total measurement uncertainty of N_2O_5 in Fig. 9. Our results remain unaffected from this correction. Furthermore, we changed $\Delta_{NO_3+N_2O_5}$ to $\Delta_{N_{NO_3+N_2O_5}}$ for the sake of consistency.

$$\Delta_{N_2O_5} = \sqrt{\left(\frac{\boldsymbol{\Delta_{N_{NO_3+N_2O_5}}}}{T^*_{N_2O_5\ \text{channel}}}\right)^2 + \left(\frac{T_{N_2O_5\ \text{channel}}\,[NO_3]\Delta_{T_{Filter}}}{T^*_{N_2O_5\ \text{channel}}}\right)^2 + \left(\frac{T_{Filter}T_{N_2O_5\ \text{channel}}\Delta[NO_3]}{T^*_{N_2O_5\ \text{channel}}}\right)^2 + \left([N_2O_5]\frac{\Delta T^*_{N_2O_5\ \text{channel}}}{T^*_{N_2O_5\ \text{channel}}}\right)^2 + \left(\frac{\boldsymbol{T_{Filter}[NO_3]\Delta T_{N_2O_5}}}{\boldsymbol{T^*_{N_2O_5\ \text{channel}}}}\right)^2}$$

References

Brown, S. S., An, H., Lee, M., Park, J.-H., Lee, S.-D., Fibiger, D. L., McDuffie, E. E., Dubé, W. P., Wagner, N. L., and Min, K.-E.: Cavity enhanced spectroscopy for measurement of nitrogen oxides in the Anthropocene: results from the Seoul tower during MAPS 2015, Faraday Discuss., 200, 529–557, https://doi.org/10.1039/c7fd00001d, 2017.

Burkholder, J. B., Sander, S. P., Abbatt, J., Barker, J. R., Cappa, C., Crounse, J. D., Dibble, T. S., Huie, R. E., Kolb, C. E., Kurylo, M. J., Orkin, V. L., Percival, C. J., Wilmouth, D. M., and Wine, P. H.: Chemical Kinetics and Photochemical Data for Use in Atmospheric Studies, Evaluation No. 19," JPL Publication 19-5, Jet Propulsion Laboratory, Pasadena, 2019.

Burkholder, J. B., Caravan, R. L., Huie, R. E., Orkin, V. L., Percival, C. J., Sander, R., Sander, S. P., and Wilmouth, D. M.: Chemical Kinetics and Photochemical Data for Use in Atmospheric Studies, Evaluation No. 20, JPL Publication 25-1, Jet Propulsion Laboratory, Pasadena, 2025.

Friedrich, N., Tadic, I., Schuladen, J., Brooks, J., Darbyshire, E., Drewnick, F., Fischer, H., Lelieveld, J., and Crowley, J. N.: Measurement of NOx and NOy with a thermal dissociation cavity ring-down spectrometer (TD-CRDS): instrument characterisation and first deployment, Atmos. Meas. Tech., 13, 5739–5761, https://doi.org/10.5194/amt-13-5739-2020, 2020.

Kennedy, O. J., Ouyang, B., Langridge, J. M., Daniels, M. J. S., Bauguitte, S., Freshwater, R., McLeod, M. W., Ironmonger, C., Sendall, J., Norris, O., Nightingale, R., Ball, S. M., and Jones, R. L.: An aircraft based three channel broadband cavity enhanced absorption spectrometer for simultaneous measurements of NO3, N2O5 and NO2, Atmos Meas Tech, 4, 1759–1776, https://doi.org/10.5194/amt-4-1759-2011, 2011.

Liebmann, J. M., Schuster, G., Schuladen, J. B., Sobanski, N., Lelieveld, J., and Crowley, J. N.: Measurement of ambient NO_3 reactivity: Design, characterization and first deployment of a new instrument, Atmos Meas Tech, 10, 1241–1258, https://doi.org/10.5194/amt-2016-381, 2017.

Nam, W., Cho, C., Perdigones, B., Rhee, T. S., and Min, K.-E.: Development of a broadband cavity-enhanced absorption spectrometer for simultaneous measurements of ambient NO_3, NO_2, and H_2O, Atmos. Meas. Tech., 15, 4473–4487, https://doi.org/10.5194/amt-15-4473-2022, 2022.

Schuster, G., Labazan, I., and Crowley, J. N.: A cavity ring down / cavity enhanced absorption device for measurement of ambient NO_3 and N_2O_5, Atmos. Meas. Tech., 2, 1–13, https://doi.org/10.5194/amt-2-1-2009, 2009.

Sobanski, N., Schuladen, J., Schuster, G., Lelieveld, J., and Crowley, J. N.: A five-channel cavity ring-down spectrometer for the detection of NO_2, NO_3, N_2O_5, total peroxy nitrates and total alkyl nitrates, Atmos. Meas. Tech., 9, 5103–5118, https://doi.org/10.5194/amt-9-5103-2016, 2016.

Türk, G. N. T. E., Andersen, S. T., Dewald, P., Schuladen, J., Lelieveld, J., and Crowley, J. N.: A small-footprint Cavity Ring-Down Spectroscopy instrument for in situ measurements of NO_3 and N_2O_5, Atmos. Meas. Tech., 19, 4815–4832, https://doi.org/10.5194/amt-19-4815-2026, 2026.

Vaughan, S., Gherman, T., Ruth, A. A., and Orphal, J.: Incoherent broad-band cavity-enhanced absorption spectroscopy of the marine boundary layer species I_2, IO and OIO, Phys. Chem. Chem. Phys., 10, 4471–4477, https://doi.org/10.1039/b802618a, 2008.

Wild, R. J., Edwards, P. M., Dube, W. P., Baumann, K., Edgerton, E. S., Quinn, P. K., Roberts, J. M., Rollins, A. W., Veres, P. R., Warneke, C., Williams, E. J., Yuan, B., and Brown, S. S.: A measurement of total reactive nitrogen, NO_y, together with NO_2, NO, and O_3 via cavity ring-down spectroscopy, Environ. Sci. Technol., 48, 9609–9615, https://doi.org/doi:10.1021/es501896w, 2014.

Reply to RC2

In the following, the referee's comments are reproduced (black) along with our replies (blue) and changes made to the text (red) in the revised manuscript. Lines numbers are referring to the unrevised version of the manuscript.

General Comments

In this paper, a new field instrument (NOyBOx) is presented which combines several commercially available instruments to measure NO, NO_2, and NO_y with custom-built, IBBCEAS cavities to measure NO_3 and N_2O_5. The instrument is well characterised and described and data from its maiden campaign is presented. The paper is well structured and data are presented clearly. Overall, I find this paper to be worthy of publication.

We thank the referee for the positive evaluation of our manuscript and for the provision of thoughtful comments.

Specific comments

1. In Section 2.2.4 it is stated that "absorption features from NO_2, H_2O and O_3 are also present; however, given their atmospheric abundances and cross-section magnitudes, only NO_2 and H_2O contribute meaningfully to the retrieved absorption". This is misleading. The Chappuis band of O_3 in the region analysed can have an equivalent or even greater overall absorption than the LOD of NO_3 under realistic conditions (20–100 ppbv). O_3 is not detectable under these conditions because the "shape" of the spectrum in this region is well approximated by a polynomial and thus absorption from O_3 is indistinguishable from the polynomial correction $p(\lambda)$. If the absorption spectrum of O_3 were more structured in this region but abundances and cross-section magnitudes remained the same, then O_3 interference would be visible. As it reads now, the passage suggests that very little light is absorbed by O_3, which is not the case; the passage should convey that the shape of the spectrum plays the key role.

We agree with the reviewer that our statement as currently phrased is misleading. Ambient ozone levels cause significant absorption between 640 and 680 nm, but the strictly monotonic behaviour of the absorption cross sections in this spectral region allows it to be accounted for within the polynomial baseline approximation. Accordingly, we now write in L247:

Within the spectral range used to monitor NO_3, absorption features from NO_2, H_2O and O_3 are also present. However, given their atmospheric abundances and cross-section magnitudes (Keller-Rudek et al., 2013), all of these contribute meaningfully to the retrieved absorption. In order to quantify NO_3 accurately, the interference by H_2O and NO_2 must be accounted for by including their absorption cross-sections in the fitting routine. The strictly monotonic behaviour of the O_3 absorption spectrum in the

considered spectral region allows its contribution to be accounted for within the polynomial baseline correction p(λ).

2. Section 2.2.1 states that the LEDs used for the NO_3 and N_2O_5 channels are cooled at different operating currents of 650mA vs 1150mA. What is the reason for such a large discrepancy; are the LEDs operated at different powers? Thermal regulation to ±0.01°C seems unrealistically good, is there data to support this?

The thermal regulation precision is claimed by the manufacturer. We have no data to support this. The different operating currents are a result from deploying two different types of LEDs in the channels. The referee is right in asking this question, there is an omission in the manuscript where only the LED for the NO_3 channel (Luminus SST-10-DR-B130) is indicated. The LED in the N_2O_5 channel is a Thorlabs model M660D2. Note however that both channels perform comparably well. We clarified this in the revised version of the manuscript by adding in L205:

In each channel, light is provided by a thermally stabilized red LED (**NO_3:** Mouser Electronics – Starboard, Luminus SST-10-DR-B130 Deep Red, max. 430 **mW; N_2O_5: Thorlabs M660D2**) with a near-Gaussian emission profile centered at 657.4 nm (FWHM 18 nm) and 660.4 nm (FWHM 21 nm) for the NO_3 (Fig. 2a, blue line) and N_2O_5 channels, respectively. Precise thermal regulation to ± 0.01 °C **(as specified by the manufacturer)** via a thermoelectric cooler (Arroyo Instruments, Laser Mount) driven by a laser diode controller (Arroyo Instruments, model 6310), at operating currents of 650 mA and 1150 mA for the NO_3 and N_2O_5 channels, suppresses wavelength drift and intensity instabilities that would otherwise corrupt the spectral baseline. **The different operating currents originate from deploying two different types of LEDs.**

3. There is significant effort given to constraining the role of water in the retrieved spectrum. This is a difficult problem for IBBCEAS systems under the stated conditions. In Fig. 2 c) H_2O is given as α while NO_3 & N_2O_5 are given as σ. Are the retrieved water concentrations from α quantitative, in other words, is the RH = 31.8% shown in Fig. 2 b) derived from the spectrum or an independent hygrometer or similar device? If it was recovered from the water contribution to the IBBCEAS spectrum, then how was this done? How do retrieved water measurements compare with hygrometer RH measurements?

The retrieved water amounts are quantitative, and the RH value in Fig. 2b comes from the IBBCEAS spectrum rather than from an independent hygrometer. The H_2O reference spectrum in Fig. 2c was recorded by sampling laboratory air shortly before the chamber experiment, and the absorption coefficient α was calculated with Eq. (1). A hygrometer in the same room gave a relative humidity of 33% at 23 °C for this reference. This is why H_2O is shown as α in Fig. 2c, whereas NO_3 and N_2O_5 are shown as cross sections σ: the water reference is an empirical spectrum of known humidity, not a literature cross section. The value of 31.8% in Fig. 2b was obtained from the spectral fit. The fitted scaling factor of the H_2O reference spectrum was multiplied by the hygrometer RH of that reference

(33%). The chamber hygrometer was not used for this value. As noted in the main text, quantifying H_2O can be problematic when the reference and sample spectra are recorded under different conditions, e.g., at different temperatures. It is feasible when the reference is freshly recorded under similar conditions, as here. To demonstrate this, we added a comparison of the CESAM hygrometer readings with the RH retrieved from the IBBCEAS spectra (new Fig. S2 in the Supplement). A linear regression gives a slope (±2σ) close to unity (1.01 ± 0.09) along with a small intercept (-1.2 %), indicating good agreement. We show the comparison in the SI (new Fig. S2) and added in L261:

To circumvent this, we use H_2O reference spectra measured in-situ in the absence of NO_3/N_2O_5 (e.g. clean daytime ambient air, laboratory air or humidified synthetic air from a chamber, Fig. 2c, grey). Since such a reference is an empirical spectrum rather than a literature cross section, it is expressed as an absorption coefficient α as derived from Eq. (1). The H_2O reference in Fig. 2c was obtained by sampling laboratory air shortly before the experiment with its humidity (33% RH at 23 °C) taken from a laboratory hygrometer reading (C2AI, Comet T7318) at the time of recording. The H_2O amount in a sample spectrum is then retrieved from the fitted scaling factor of this reference; for example, the 31.8% RH in Fig. 2b is the scaling factor multiplied by the reference RH. This approach is quantitative only if the reference is recorded shortly beforehand under conditions (in particular temperature) similar to those of the sample. Under such conditions, the retrieved RH agrees well with the CESAM chamber hygrometer (Vaisala HMP234) during this experiment, as suggested by a linear regression analysis yielding a slope (±2σ) close to unity (1.01 ± 0.09, Fig. S2). While CEAS principally allows simultaneous retrieval of multiple species in the general case (Nam et al., 2022), accurate quantification of NO_2 and H_2O can be impeded by potential residual NO_2 in the reference or variability in H_2O relative band intensities in our approach, especially when reference and sample conditions differ.

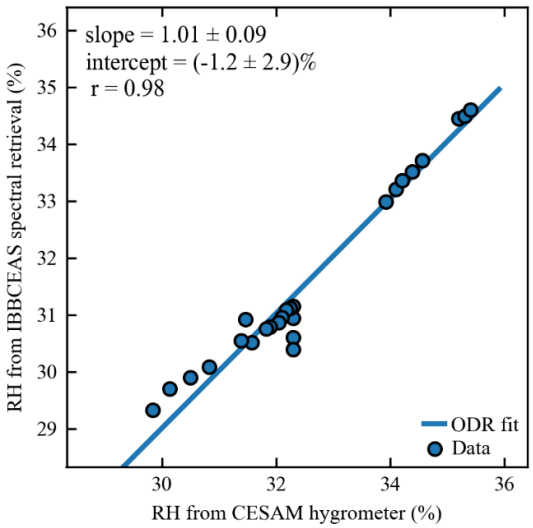


Figure S2. Relative humidity (RH) retrieved from the IBBCEAS spectra compared with the RH measured by the hygrometer of the CESAM chamber. The solid line is an orthogonal distance regression (ODR) of the IBBCEAS-retrieved RH on the hygrometer RH. The fit gives a slope of 1.01 ± 0.09 and an intercept of (−1.2 ± 2.9) %RH, where the uncertainties are two standard errors; the Pearson correlation coefficient is $r = 0.98$. The slope is consistent with unity within the fit uncertainty, and the IBBCEAS retrieval is on average 1 %RH lower than the hygrometer over the sampled range (about 30–35 %RH).

4. How well do NO_2 concentrations retrieved from the IBBCEAS system quantitatively agree with the CAPS measurements in NOyBOx? Since retrieved NO_2 is important for accurate NO_3 retrieval, it would be enlightening to see this data. Can NO_2 concentrations be fully constrained by the CAPS instrument? This is an advantage of an integrated instrument that should be elaborated upon.

The empirical H_2O reference spectra we record usually contain a residual NO_2 contribution. In addition, NO_2 and H_2O share intense absorption features at 647 nm. A quantitative agreement with the CAPS measurement is therefore not expected in field data. Furthermore, NO_2 is included as a fit component in our retrieval procedure because its absorption overlaps spectrally with NO_3 and H_2O; it is not intended as a quantitative NO_2 measurement. For accurate NO_3 quantification, what matters is that the NO_2 absorption structure is represented in the fit, not the accuracy of the retrieved NO_2 amount. This is demonstrated with the synthetic spectra analysis in Section 3.5, suggesting a mean NO_3 retrieval bias of only ±7% and ±10% for the NO_3 and N_2O_5 channel, respectively. As demonstrated in our new Figure S6, we found from this analysis that despite NO_2 quantification being highly biased in the presence of high H_2O concentrations, the NO_2 bias is only weekly correlated to the NO_3 bias, with Pearson correlation coefficients r of –0.32 (NO_3 channel) and +0.34 (N_2O_5 channel). Nevertheless, we agree that the co-located CAPS NO_2 measurement is an advantage of the integrated instrument. It provides an independent constraint on NO_2 that can be used to limit the crosstalk between the H_2O and the NO_2 contribution to the fit to some extent. Note however that fixing NO_2 to the CAPS value changes the retrieved NO_3 by less than 0.5% for the example shown in Fig. 2.

We added in L264:

As discussed below with a synthetic spectra analysis (see section 3.5), for accurate NO_3 quantification, what matters is that the NO_2 and H_2O absorption structures are represented in the fit, not the accuracy of the retrieved NO_2 amount: While NO_2 quantification is strongly biased in the presence of water, the NO_3 retrieval accuracy is only marginally impacted. An example fit along with the retrieved concentrations is shown in Fig. 2b (blue line) for a mixture $NO_3/NO_2/H_2O$ generated in CESAM simulation chamber (https://www.cesam.cnrs.fr/). **Note that in this example fit, constraining NO_2 to the CAPS measurement (17.9 ppbv) would alter the retrieved NO_3 amount by less than 0.5%.**

In L268, we wrote:

In this routine, NO_3 is the target species; NO_2 and H_2O are fitted mainly to account for their spectral interference, and their retrieved amounts are subject to larger uncertainty.

We added Fig. S5 to the Supplement and write in L457:

The synthetic spectra also show an RH-dependent NO_2 bias (Fig. S5, Supplement), which increases approximately linearly with RH by 0.20 (NO_3 channel) and 0.33 ppbv per % RH (N_2O_5 channel). For NO_3 above the LOD, this NO_2 bias is only weakly correlated with our above-mentioned NO_3 biases (r = –0.36 and +0.32 for the N_2O_5 and NO_3 channel, respectively), thereby confirming the low sensitivity of the NO_3 retrieval accuracy to NO_2 quantification. Nevertheless, taking advantage of the instrument's

integrated CAPS analyzer, constraining NO_2 in the fit to measured values may allow reduction of the retrieval bias in both channels – especially under very humid conditions.

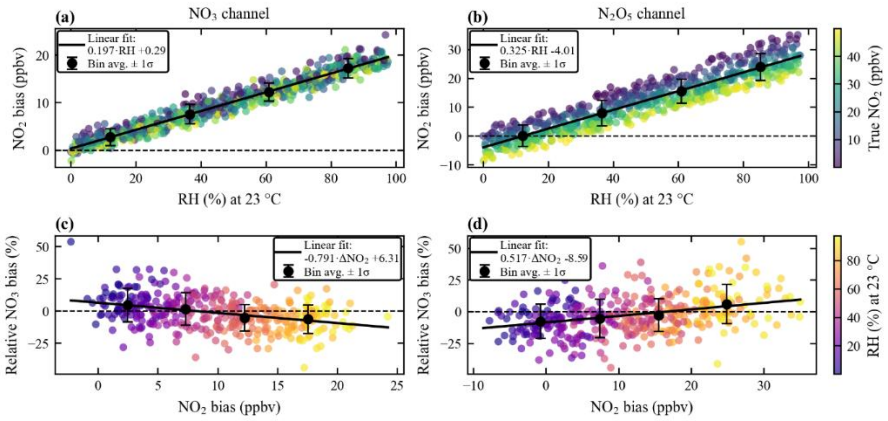


Figure S5. Systematic NO_2 retrieval bias and its effect on the retrieved NO_3 for the NO_3 cavity (left; a, c) and the N_2O_5 cavity (right; b, d), based on Latin hypercube–sampled synthetic spectra ($N = 600$ sampled points, each averaged over 10 Monte Carlo noise realisations, so the biases shown are systematic and less random). (a, b) Absolute NO_2 bias (retrieved − true, ppbv) as a function of relative humidity at 23 °C, coloured by the true NO_2 mixing ratio. (c, d) Relative NO_3 bias (%) as a function of the NO_2 bias (ppbv), coloured by relative humidity; only points with a true NO_3 above the noise-based limit of detection are shown, because the relative bias diverges for small NO_3. Black circles with error bars denote bin averages (four quantile bins) ± 1σ of the within-bin scatter, solid black lines are linear fits through the bin averages (parameters given in the legends), and dashed lines mark zero bias. Colour scales are identical for both cavities. In both cavities, the NO_2 bias increases with RH; in the N_2O_5 cavity it is additionally larger at low NO_2. Over the sampled NO_2 (0–50 ppbv) and RH (0–100 %) ranges, this NO_2 bias is weakly correlated to the retrieved NO_3, with Pearson correlation coefficients of –0.32 and +0.34 in the NO_3 and N_2O_5 cavities, respectively.

5. Is the temperature used in Fig. 9 b) the ambient temperature of the sample air before entering the instrument or after leaving the unheated cavity? What is the internal temperature of the instrument / gas stream within the cavity? It is suggested in Section 3.5.1 that degradation of the NO_3 signal in the Allan plot is "likely reflecting the absence of temperature regulation in the NO_3 cavity". More information on the internal temperature of the instrument is required to support this claim. It is also important for understanding the "true" ambient concentrations of NO_3 and N_2O_5; if the gas gets warmed up in the inlet and within the instrument, it will have an effect on the measurement by disturbing the thermal equilibrium.

We thank the reviewer for emphasizing the potential effects of cavity temperature on (1) the Allan deviation and (2) the quantification of ambient NO_3 levels. Regarding the Allan deviation analysis, the internal NO_3 cavity temperature increased by 0.6 °C, from 20.7 °C to 21.3 °C, during the period over which the data were collected. While the cavities and their alignment are certainly sensitive to temperature, other effects causing drift over longer time scales, such as changes in mirror reflectivity, may also contribute to our observations. We have accordingly rephrased our statement in L425 to make it more cautious:

Above 10 s, the two channels diverge: the N_2O_5 channel remains stable up to 100 s, whereas drift degrades the NO_3 channel LOD beyond 30 s. During the data acquisition period, the internal NO_3 cavity

temperature increased by 0.6 °C. While the absence of temperature regulation in the NO_3 cavity may lead to temperature-induced misalignment, potentially explaining its lower long-term stability compared to the thermostated N_2O_5 cavity, other sources of slow instrumental drift may also contribute to this observation.

Regarding the ambient measurements in Fig. 9: Panel (b) shows the ambient temperature, i.e. before entering the cavity. In this example, the internal cavity temperature is on average 5 K higher than ambient temperature. We used our box model introduced in Section 3.3. to account for the additional NO_3 formed from thermal dissociation of N_2O_5 when sampling through the cavity. Due to the short residence time, correction factors were small, ranging from 0.91 to 0.99 (median: 0.94). We added a new plot to the SI (Fig. S7) showing uncorrected NO_3 values along with corrected NO_3, the fractional correction in % and the difference between cavity and ambient temperature.

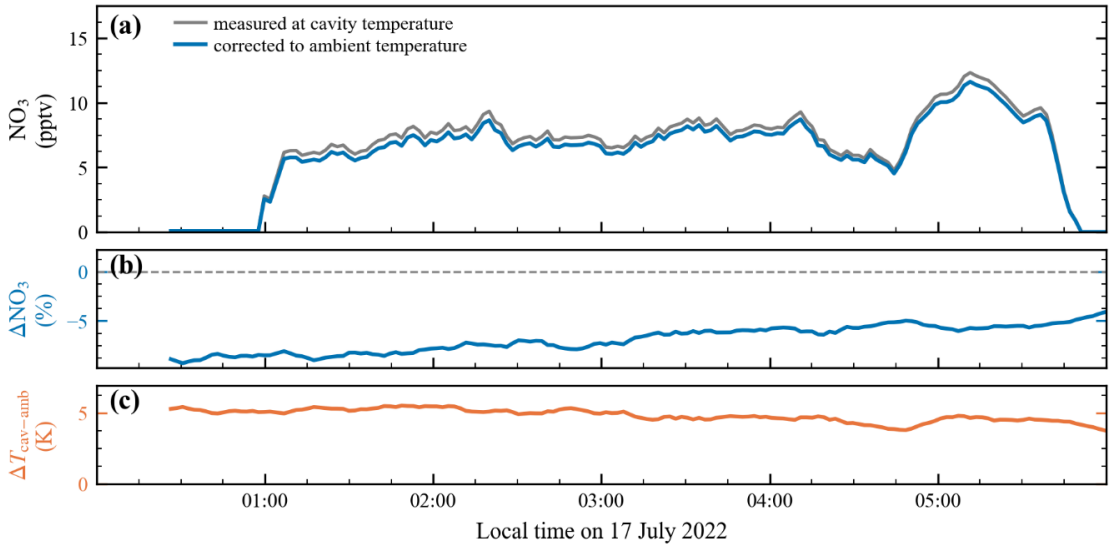


Figure S7. Correction of the measured NO_3 mixing ratio for the thermal shift of the NO_3–NO_2–N_2O_5 equilibrium in the cavity, for the night of 17 July 2022 (00:00–06:00 LT). (a) NO_3 as measured at cavity temperature (grey) and after correction to ambient temperature (blue). (b) Relative alteration of NO_3 caused by the correction, $\Delta NO_3 = (NO_{3,corr} - NO_{3,meas}) / NO_{3,meas}$. (c) Gas temperature difference between the cavity and ambient air (40 m), $\Delta T = T_{cav} - T_{amb}$. The correction factor was obtained using the box model used in section 3.3 for each data point by explicitly simulating the NO_3/N_2O_5 kinetics along the sampling line, starting from ambient equilibrium. The gas was assumed to be at ambient temperature until it entered the cavity, where it immediately reaches cavity temperature (residence time 1.3 s, pressure 970 mbar). It included an NO_3 wall loss of 0.1 s^{-1} in the cavity and a filter transmission of 0.9 for NO_3.

We added in L284:

When the NO_3 cavity temperature strongly differs from ambient temperature, NO_3 levels must be corrected to account for the shift in the highly temperature-dependent NO_2-NO_3-N_2O_5 equilibrium (reactions R2 and R3) during the residence time in the cavity.

In L515, we added:

NO_3 levels were additionally corrected by a factor of 0.94 on average using our box model introduced in Sect. 3.3. This accounts for NO_3 formed by N_2O_5 dissociation (R3) during the residence time in the cavity, which was ca. 5 K warmer than ambient air (see Fig. S7, Supplement).

6. Regarding the “calibration” mode outlined in section 2. It is stated that during calibration “excess gas of the NO_3 and N_2O_5 channels is vented through sampling inlets” with no mention of scrubbing. Is it correct that some flow of 800 ppbv NO_2 is vented into ambient air through the NO_3 / N_2O_5 inlet? Is the performance of the MFC at the exit of the cavity affected by the high levels of NO_2 flowing through it?

Our sentence as currently phrased is misleading. For reasons outlined in our response to comment 7, the N_2O_5 channel is vented through the scrubbed overflow (OFL), while the NO_3 channel is mainly vented through the sampling inlet. To avoid contamination of ambient air with such high NO_2 concentrations, we manually equip the NO_3 cavities’ sampling inlet with a charcoal cartridge during the calibration period. No NO_2 is vented into ambient air at any time. The mass flow indicated by the controller agrees with that by a flowmeter (TSI, model 4140), thereby confirming that the MFC provides accurate mass flows despite regular exposure to high NO_2 mixing ratios. We corrected our manuscript accordingly and write in L152:

Excess gas in the latter is vented via its own sampling inlet, whereas a dedicated overflow outlet (OFL) is used for the former. In both cases, the corresponding vents are equipped with removable charcoal cartridges to prevent the release of calibration gases into the ambient air.

7. Regarding Fig. 1

a. Why is there a tee fitting at the junction between the inlet, ZA / NO_2 gas, and the cavity for the NO_3 channel, but a 3-way valve in the same position in the N_2O_5 channel?

The different implementation reflects the hardware available when the channels were built rather than a difference in function. The two configurations are functionally equivalent. In both channels, the calibration/zero-air gas is supplied at a flow rate exceeding the cavity’s sample flow, so that the excess exits either through the dedicated overflow (OFL) or through the sampling inlet. This excludes ambient air from the cavity during calibration and zero measurements. In the NO_3 channel, this is achieved with a tee fitting combined with a two-way valve on the calibration line: when the valve is open, the calibration gas overflows the inlet, and when it is closed, the cavity samples ambient air. In the N_2O_5 channel, the same function is performed by a three-way valve but vented through the OFL since the port to the sampling line is blocked. We have not observed any difference in performance, as the overflow ensures that in both cases the cavities sample only calibration gas when the corresponding valve is open/switched.

b. What type of 3-way valves are used, and are they all the same? Do the valves switch between a mode where all ports are open and a mode where one port is closed or do the valves switch between two modes where a different port is closed (i.e. all ports cannot be open at the same time)? It would be helpful to state this explicitly. It would also be helpful for understanding the diagram to mark on the diagram which outlets/inlets are common / always open.

We use 3/2-way (Bürkert, type 0121, no. 20063588) and 2-way (Bürkert, type 0121, no. 77191) solenoid valves. The 3/2-way valves switch between two modes allowing the cavity to sample either ambient air

or ZA/NO_2, i.e. all ports cannot be open at a time. We agree with the reviewer that marking the ports will increase the clarity of Fig. 1.

c. Are the valves in the sample line made of an inert material or coated in one?

The valves consist of chemically inert PTFE.

For clarification, we coloured the ports of the valves in Fig. 1 according to the modes during which they are active (brown: calibration, blue: background, purple: sampling, grey: always open), updated the figure caption and added in L155:

The mode switching in the commercial analyzer subsystem and the N_2O_5 channel is enabled by 3/2-way solenoid valves consisting of PTFE (Bürkert, type 0121, no. 20063588), while a 2-way solenoid PTFE valve (Bürkert, type 0121, no. 77191) in combination with a Perfluoroalkoxy alkane (PFA) T-piece (Swagelok, PFA-420-3) is used in the NO_3 channel for reasons of hardware availability.

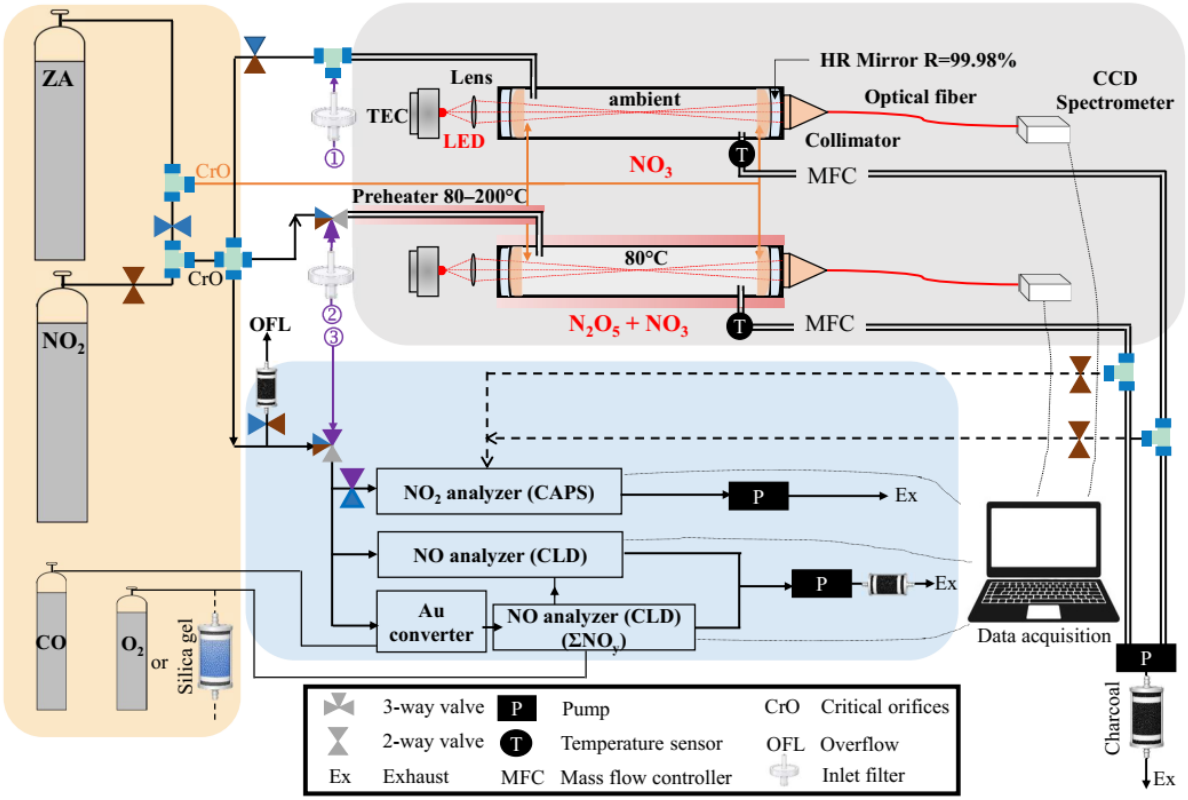


Figure 1. Schematic diagram of the NOyBOx instrument. The two custom-built IBBCEAS subsystems with separate inlets 1 and 2 is shaded grey. The commercial analyzer subsystem for NO, NO_2, and total gas-phase NO_y is shaded blue and share inlet 3. The gas supply assembly for purging (orange solid lines), background and calibration measurements is marked in orange. **The valves are coloured according to the modes (blue: background, brown: calibration, purple: sampling, grey: always open) they are active in.** The black dashed lines show how the cavity exhaust flow is coupled to the NO_2 analyser during calibration periods. **Note that the NO_3 channel's inlet is equipped with an additional charcoal filter (not shown) when calibrated with NO_2.**

Technical Corrections

Fig. 9 b) legend should read Burkholder et al.

Correction made.

Fig. 9 c) has an inconsistency between the labels and the legend. Either NO_3 should be black on the axis label and included in the legend or there should be no legend and the N_2O_5 + NO axis labels should be coloured appropriately.

Correction made.

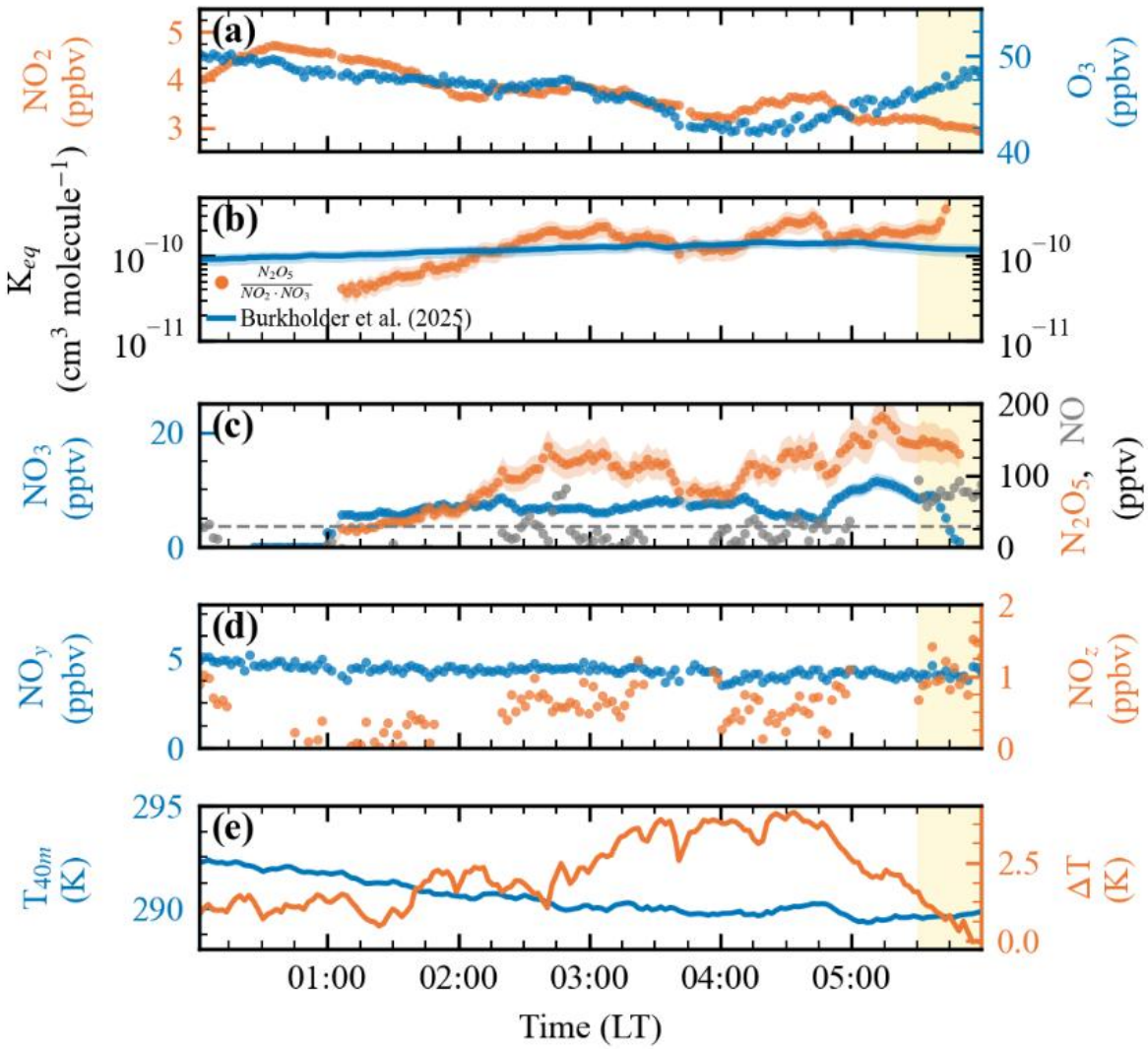


Figure 9. Nocturnal time series during the ACROSS campaign (16–17 July 2022, 00:00–06:00 LT); yellow shading indicates sunrise (05:30 LT). (a) NO_2 (orange, left axis) and O_3 (blue, right axis). (b) Measured NO_3–N_2O_5–NO_2 relationship $[N_2O_5]/([NO_2][NO_3])$ (orange), compared with the evaluated, temperature-dependent equilibrium constant from Burkholder et al. (2025) (blue line, shading = uncertainty). (c) NO_3 (blue, left axis) and N_2O_5 (orange, right axis) mixing ratios with the total measurement uncertainty (shading), alongside NO (gray, right axis, provided py IMT Nord Europe); the dashed line marks the NO detection limit (30 pptv). (d) NO_y (blue, left axis) and NO_z (orange, right axis). (e) Ambient temperature at 40 m (blue, left axis) and the temperature difference ΔT between 5 m and 41 m (orange, right axis) from CNRM (Météo-France).

Additional changes to the manuscript

1. The recommendation for the NO_3–NO_2–N_2O_5 equilibrium constants has been re-evaluated recently in Burkholder et al. (2025), while we still used the outdated expression in Burkholder et al. (2019). We updated K_{eq} in Fig. 9 and the literature list accordingly.
2. The work by (Türk et al., 2026) is no longer a preprint, but published in AMT. We updated the reference in the literature list accordingly.
3. In L326, we added the unit of the slope for clarification: Linear regression (solid lines) of the reflectivity yielded (1.18 ± 1.58) x 10^{-8} nm^{-1} x λ + 99.987% and (4.81 ± 0.75) x 10^{-8} nm^{-1} x λ + 99.949%.
4. We accidently omitted the fifth term propagating the error of $T_{N_2O_5}$ in Eq. (6). We corrected the equation accordingly. Note however that we used the correct version of Eq. (6) to calculate the total measurement uncertainty of N_2O_5 in Fig. 9. Our results remain unaffected from this correction. Furthermore, we changed $\Delta_{NO_3+N_2O_5}$ to $\Delta_{N_{NO_3+N_2O_5}}$ for the sake of consistency.

$$\Delta_{N_2O_5} = \sqrt{\left(\frac{\boldsymbol{\Delta_{N_{NO_3+N_2O_5}}}}{T^*_{N_2O_5\ \text{channel}}}\right)^2 + \left(\frac{T_{N_2O_5\ \text{channel}}\,[NO_3]\Delta_{T_{Filter}}}{T^*_{N_2O_5\ \text{channel}}}\right)^2 + \left(\frac{T_{Filter}T_{N_2O_5\ \text{channel}}\Delta[NO_3]}{T^*_{N_2O_5\ \text{channel}}}\right)^2 + \left([N_2O_5]\frac{\Delta T^*_{N_2O_5\ \text{channel}}}{T^*_{N_2O_5\ \text{channel}}}\right)^2 + \left(\frac{\boldsymbol{T_{Filter}[NO_3]\Delta T_{N_2O_5}}}{\boldsymbol{T^*_{N_2O_5\ \text{channel}}}}\right)^2}$$

References

Burkholder, J. B., Sander, S. P., Abbatt, J., Barker, J. R., Cappa, C., Crounse, J. D., Dibble, T. S., Huie, R. E., Kolb, C. E., Kurylo, M. J., Orkin, V. L., Percival, C. J., Wilmouth, D. M., and Wine, P. H.: Chemical Kinetics and Photochemical Data for Use in Atmospheric Studies, Evaluation No. 19," JPL Publication 19-5, Jet Propulsion Laboratory, Pasadena, 2019.

Burkholder, J. B., Caravan, R. L., Huie, R. E., Orkin, V. L., Percival, C. J., Sander, R., Sander, S. P., and Wilmouth, D. M.: Chemical Kinetics and Photochemical Data for Use in Atmospheric Studies, Evaluation No. 20, JPL Publication 25-1, Jet Propulsion Laboratory, Pasadena, 2025.

Nam, W., Cho, C., Perdigones, B., Rhee, T. S., and Min, K.-E.: Development of a broadband cavity-enhanced absorption spectrometer for simultaneous measurements of ambient NO_3, NO_2, and H_2O, Atmos. Meas. Tech., 15, 4473–4487, https://doi.org/10.5194/amt-15-4473-2022, 2022.

Türk, G. N. T. E., Andersen, S. T., Dewald, P., Schuladen, J., Lelieveld, J., and Crowley, J. N.: A small-footprint Cavity Ring-Down Spectroscopy instrument for in situ measurements of NO_3 and N_2O_5, Atmospheric Measurement Techniques, 19, 4815–4832, https://doi.org/10.5194/amt-19-4815-2026, 2026.